CrystEngComm

ROYAL SOCIETY OF CHEMISTRY

PAPER

View Article Online
View Journal | View Issue

Cite this: *CrystEngComm*, 2023, **25**, 284

MOF-on-MOF heterostructures with core–shell and core–satellite structures *via* controllable nucleation of guest MOFs†

Shumin Li,[a] Liang Zhao,*[a] Yining Yao,[a] Zhengying Gu,[a] Chao Liu,[a] Wenli Hu,[a] Ye Zhang,[a] Qian Zhao[a] and Chengzhong Yu *[ab]

Received 15th September 2022,
Accepted 25th November 2022

DOI: 10.1039/d2ce01272c

rsc.li/crystengcomm

The integration of two or more different types of metal–organic frameworks (MOFs) into hybrid MOF-on-MOF heterostructures has been widely studied, and the diversity of MOF-on-MOF heterostructures can be effectively increased by exploring the integration strategy of different MOF building blocks. Here, we report the structure regulation of MOF-on-MOF hybrids *via* controlling the heterogeneous nucleation and homogeneous nucleation growth of guest MOFs. By using ZIF-90 as the host and ZIF-8 as the guest, binary ZIF-90@ZIF-8 complexes can be synthesized. Moreover, the nucleation mode of ZIF-8 depends on the addition sequence of metal ions and ligands of the guest MOF, including heterogeneous nucleation and homogeneous nucleation. Therefore, ZIF-90@ZIF-8 hybrids with a core–shell structure and smooth surface or a core–satellite structure and rough surface are successfully prepared, increasing the structural diversity of MOF-on-MOF materials.

Introduction

Metal organic frameworks (MOFs) are a family of porous materials constructed by connecting metal ions/clusters with bidentate/polydentate organic ligands.[1–3] With large specific surface areas, high pore volumes and tunable structures, MOF-based materials have been applied in many fields, including catalysis, gas adsorption/separation/storage, nonlinear optics, sensing and detection, and biomedical applications.[1–7] Particularly, MOFs in nanoparticle forms for biomedicine have become a rapidly developing hot research topic.[8–10] Compared to traditional MOFs with larger particle sizes, MOF nanoparticles possess additional advantages, *e.g.*, enhanced biological activity and chemical/colloidal stability.[11–13] In recent years, an intriguing MOF-on-MOF hybridization design has received special attention *via* integration of two or more different types of MOFs in one composite.[14–16] The MOF-on-MOF design can enrich not only the composition (*e.g.* ligands and/or metal centers) but also the structural diversities (*e.g.* pore sizes, surface properties and functions) of MOFs.

Zeolitic imidazolate frameworks (ZIFs) are considered as a subcategory of MOFs and have been developed rapidly since they combine the properties of both MOFs and zeolites, and have high thermal stability.[17] Among various ZIFs, ZIF-8[18] is one of the most popular members and has attracted great attention in catalysis,[19–21] adsorption and separation,[22] and electrochemistry.[23] In parallel, ZIF-90 has gained increasing research interest as it contains a reactive aldehyde group in the framework with ease of further functionalization.[24,25] Recently, Mo and co-workers reported ZIF-8@ZIF-90 as advanced fluorescence-encoding materials.[26] However, the synthesis of ZIF-90@ZIF-8 has not been reported. Moreover, MOF-on-MOF binary compositions can be adjusted into core–shell, core–satellite, yolk–shell, hollow multi-shell, asymmetric and film architectures[27] *via* various strategies.[28–31] For example, Oh's group prepared MOF-on-MOFs with core–shell-type and semitubular morphologies, using the same host MOF and different guest MOFs.[28] Liu and co-workers synthesized MOF-on-MOF heterostructures with the growth sites of guest MOFs determined by host MOFs with different morphologies.[29] Nevertheless, it has been rarely reported that the architecture of MOF-on-MOFs can be regulated using one host MOF with the same morphology and the same type of guest MOF.

Here, by using ZIF-90 as the host and ZIF-8 as the guest, binary ZIF-90@ZIF-8 complexes with core–shell and core–satellite structures were synthesized for the first time. As shown in Fig. 1, the structures of the hybrids can be regulated by controlling the heterogeneous nucleation and

[a] *School of Chemistry and Molecular Engineering, East China Normal University, Shanghai 200241, P. R. China. E-mail: lzhao@chem.ecnu.edu.cn, czyu@chem.ecnu.edu.cn*
[b] *Australian Institute for Bioengineering and Nanotechnology, The University of Queensland, Brisbane, Queensland 4072, Australia. E-mail: c.yu@uq.edu.au*
† Electronic supplementary information (ESI) available. See DOI: https://doi.org/10.1039/d2ce01272c

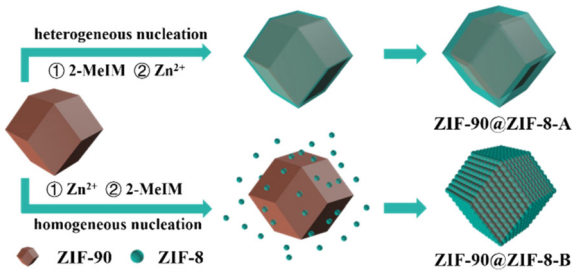

Fig. 1 Schematic illustration of the synthesis of ZIF-90@ZIF-8.

homogeneous nucleation growth of the guest MOF, simply *via* changing the addition sequence of metal ions and ligands of the guest MOF during the synthesis. When 2-MeIM is introduced before Zn^{2+}, the heterogeneous nucleation and growth of ZIF-8 on ZIF-90 core particles lead to ZIF-90@ZIF-8-A with a core–shell structure and smooth surface. When Zn^{2+} is added first, ZIF-8 nanoparticles tend to form *via* homogeneous nucleation in solution, then conjugate with ZIF-90 and generate ZIF-90@ZIF-8-B with a core–satellite structure and rough surface. Different from studies where using host MOFs with different morphologies or different types of guest MOFs are necessary, the structural regulation involves the same host–guest pair in our strategy (ZIF-90 rhombic dodecahedron–ZIF-8).

Experimental

Chemicals and materials

Zinc nitrate hexahydrate ($Zn(NO_3)_2{\cdot}6H_2O$, 98%) and dimethylacetamide (DMAC, 99%) were purchased from Sinopharm Chemical Regent Co., Ltd. Zinc acetate ($Zn(CH_3COO)_2$, 99.5%, Adamas-beta), imidazole-2-carboxyaldehyde (2-ICA, 98%, Adamas-beta), 2-methylimidazole (2-MeIM, Aldrich) and methanol (AR, 99%, Adamas-beta) were used as received. Deionized water was used in all experiments (Milli-DI Water Purification System).

Synthesis of ZIF-90

ZIF-90 nanoparticles were prepared according to a literature protocol with slight modification.[32] In a typical synthesis, 2-ICA (1.922 g, 20 mmol) was added to 25 mL of DMAC and heated to 80 °C until 2-ICA was completely dissolved. Then, the solution was cooled to room temperature before adding 25 mL of $Zn(NO_3)_2{\cdot}6H_2O$ (595 mg, 2 mmol) in DMAC, followed by stirring at 30 °C for 4 h. Afterwards, 50 mL of methanol was added to the mixture and stirred for another 5 min. Finally, the mixture was aged for 25 min, and the formed particles were separated by centrifugation and washed with methanol five times.

Synthesis of ZIF-90@ZIF-8-A

To synthesize the ZIF-90@ZIF-8-A heterostructure, 3 mg of ZIF-90 was dispersed in 6 mL of methanol solution, and then 3 mL of 80 mM 2-MeIM methanol solution was added to the solution under stirring at room temperature. After stirring for 5 min, 3 mL of 20 mM $Zn(NO_3)_2{\cdot}6H_2O$ methanol solution was added. Then, the mixture was allowed to react for 2 h under stirring before aging for another 12 h. The final product was collected by centrifugation, and washed with methanol three times. This sample was named as ZIF-90@ZIF-8-A.

Synthesis of ZIF-90@ZIF-8-B

To synthesize the ZIF-90@ZIF-8-B heterostructure, 3 mg of ZIF-90 was dispersed in 6 mL of methanol solution, and then 3 mL of 20 mM $Zn(NO_3)_2{\cdot}6H_2O$ methanol solution was added to the solution under stirring at room temperature. After stirring for 5 min, 3 mL of 80 mM 2-MeIM methanol solution was added. The mixture was allowed to react for 2 h under stirring before aging for another 12 h. The final product was collected by centrifugation, washed with methanol three times, and named as ZIF-90@ZIF-8-B.

Synthesis of ZIF-8

ZIF-8 nanoparticles were prepared following a reported method.[33] 1.8 mmol of zinc acetate and 18.0 mmol of 2-methylimidazole were each individually dissolved in 12 mL of methanol for 1 h. The two prepared solutions were mixed and stirred for 10 min, followed by sonication for 1 min. Then, the mixed solution was immersed in an oil bath at 70 °C for 10 min. The solution was allowed to cool to room temperature and the resultant ZIF-8 particles were collected by centrifugation and washed three times with methanol.

Characterization

Scanning electron microscopy (SEM) images were acquired using a scanning electron microscope (HITACHI-S4800). Transmission electron microscopy (TEM) images were obtained with a Hitachi HT7700. X-ray diffraction (XRD) patterns were recorded using a Smartlab SE X-ray diffractometer with Cu Kα radiation (λ = 0.154 nm). The Fourier transform infrared (FTIR) spectra of samples were collected on a Thermo Fisher FT-IR-Nicolet IS50 by the attenuated total reflectance method.

Results and discussion

In our synthesis, ZIF-90 nanoparticles with a regular morphology were firstly synthesized as the host. SEM (Fig. 2a) and TEM (Fig. 2b) images of ZIF-90 both show nanoparticles with a rhombic dodecahedral shape. The nanoparticles have a uniform size of about 225 nm and a smooth surface. The XRD pattern of ZIF-90 in Fig. 3a shows six main peaks at 7.46, 10.52, 12.86, 14.86, 16.60 and 18.18°, which can be indexed to the (0 1 1), (2 0 0), (1 1 2), (0 2 2), (0 1 3) and (2 2 2) diffractions. The results are consistent with the simulated patterns of ZIF-90,[34] indicating that crystalline ZIF-90 nanoparticles were successfully prepared.

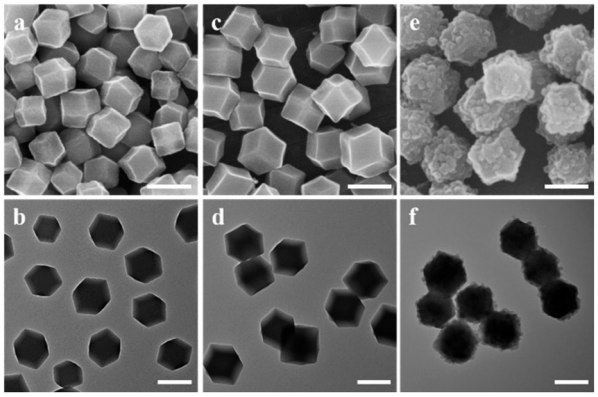

Fig. 2 SEM (a, c and e) and TEM (b, d and f) images of (a and b) ZIF-90, (c and d) ZIF-90@ZIF-8-A, (e and f) ZIF-90@ZIF-8-B. The scale bar is 200 nm.

Then, using ZIF-90 nanoparticles as the host, ZIF-90@ZIF-8-A and B heterostructures were synthesized (Fig. 1). SEM (Fig. 2c) and TEM (Fig. 2d) images reveal that ZIF-90@ZIF-8-A shows a well-defined rhombic dodecahedral morphology with a smooth surface and uniform size distribution, similar to that of the host ZIF-90. However, the average diameter of ZIF-90@ZIF-8-A is increased to 278 nm, indicating the heterogeneous nucleation and growth of ZIF-8 on ZIF-90. In contrast, ZIF-90@ZIF-8-B shows a rough surface as evidenced from SEM (Fig. 2e) and TEM (Fig. 2f) images, different from ZIF-90@ZIF-8-A with a smooth surface. The average size of ZIF-8 nanoparticles is estimated to be ~25–30 nm in diameter.

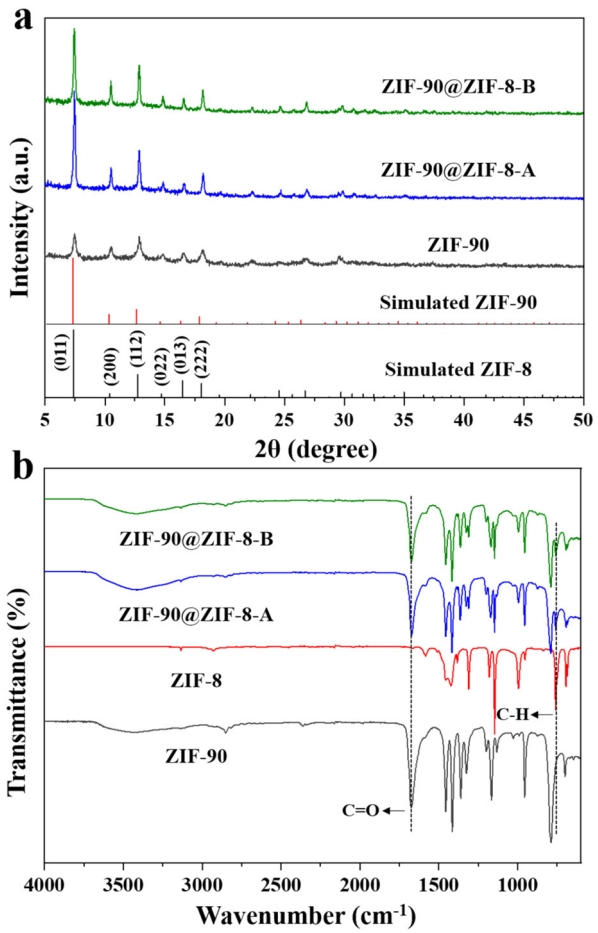

Fig. 3 (a) XRD spectra and (b) FTIR spectra of ZIF-90, ZIF-8, ZIF-90@ZIF-8-A and ZIF-90@ZIF-8-B.

The XRD patterns of the synthesized ZIF-90@ZIF-8-A and ZIF-90@ZIF-8-B nanoparticles are shown in Fig. 3a. It is noted that due to the isostructural nature of ZIF-90 and ZIF-8, the XRD patterns of all the particles, including ZIF-90@ZIF-8-A, ZIF-90@ZIF-8-B, ZIF-90 and ZIF-8, showed diffractions at the same positions except for slight differences in relative intensity. It is noted that both ZIF-8 and ZIF-90 have zinc atoms, and their compositional difference is in the ligands. In ZIF-8, the ligand 2-MeIM does not contain oxygen, in contrast to 2-ICA in ZIF-90 which contains an aldehyde group. To provide information on the composition distribution in the binary MOF composites, high-angle annular dark-field scanning transmission electron microscopy (HAADF-STEM) and elemental mapping (Zn and O) images of ZIF-90@ZIF-8-A were taken as an example, using ZIF-90 as a control sample. In the case of ZIF-90, from the HAADF-STEM image (Fig. S1a†), Zn and O mappings (Fig. S1b†) and the superimposed elemental image (Zn + O, Fig. S1c†), Zn and O are evenly distributed over the entire nanoparticle range. However, for ZIF-90@ZIF-8-A (Fig. S1d–f†), a Zn-rich outer layer (red color) is evident in comparison with ZIF-90, consistent with the ZIF-8 layer formed on the outer surface of ZIF-90 in the ZIF-90@ZIF-8-A heterostructure.

To further differentiate ZIF-90 and ZIF-8 in the composites, the FTIR spectra of the two ZIF-90@ZIF-8 nanoparticles and ZIF-90 were also recorded. In addition, ZIF-8 nanoparticles were synthesized and used in the FTIR study to verify the successful modification of ZIF-8 on the ZIF-90 surface. As shown in the TEM images (Fig. S2a and b†), ZIF-8 with an estimated particle size of about 300 nm was synthesized. The XRD pattern of ZIF-8 is consistent with the simulated result, further confirming the successful synthesis of ZIF-8 (Fig. S3†).[35] From the FTIR spectra (Fig. 3b), both ZIF-90@ZIF-8 composites display one band at around 1675 cm^{-1} corresponding to the C=O stretching of 2-ICA (also observed in ZIF-90),[24] and another peak at 759 cm^{-1} originating from the stretching vibration of the C–H group in 2-MeIM (also observed in ZIF-8).[36] Collectively, the XRD, SEM, TEM and FTIR results indicate that core–shell structure ZIF-90@ZIF-8-A with a smooth surface and core–satellite structure ZIF-90@ZIF-8-B with a rough surface have been successfully synthesized.

The ZIF-90@ZIF-8 hybrids with core–shell and core–satellite structures obtained in our work are unique in composition compared with reported MOF-on-MOFs with core–shell structures such as ZIF-8@ZIF-67,[37] Fe-MIL-88B@Fe-MIL-88C[31] and IRMOF-3@MOF-5,[38] or MOF-on-MOFs with core–satellite structures such as MIL-125@ZIF-8,[29] PCN-222@PCN-608, PCN-222@NU-1000, PCN-222@PCN-134, Zr-BTB@PCN-134,[30] and MIL-88B@UIO-66.[39] Although the composition of ZIF-90@ZIF-

8 is identical to that of reported ZIF-8@ZIF-90,[26] the spatial arrangement is different which could have implications for future applications. For example, it is well known that ZIF-90 is relatively hydrophilic while ZIF-8 is hydrophobic.[40,41] It can be inferred that the surface hydrophilicity/hydrophobicity of ZIF-90@ZIF-8 and ZIF-8@ZIF-90 could be different due to the nanostructure difference. Moreover, the structural regulation of the same host–guest pair (ZIF-8 on rhombic dodecahedron ZIF-90) has been achieved in our work, leading to core–shell and core–satellite structures. This is also different from a reported ZIF-8@ZIF-90 with only a core–shell structure,[26] or other reports of MOF-on-MOFs with core–satellite structures by changing the type and morphology of the host MOF.[28,29]

To understand the formation mechanism of the ZIF-90@ZIF-8-A and ZIF-90@ZIF-8-B heterostructures, the intermediate structures at different reaction time points were monitored. In the case of ZIF-90@ZIF-8-A, a 2-MeIM solution was firstly added into a ZIF-90 solution and stirred for 5 min before Zn^{2+} addition (Fig. 4a). The reaction time was counted after the addition of Zn^{2+} precursors. The rhombic dodecahedral morphology is well kept at reaction times of 2, 5 and 20 min as confirmed by TEM observations (Fig. 4b–d). However, the average diameters of nanoparticles gradually increased to 24 nm, 31 nm and 41 nm at 2, 5, and 20 min, respectively. This observation indicates that by adding 2-MeIM first and then Zn^{2+} to react with ZIF-90, a layer of ZIF-8 is selectively grown on the surface of ZIF-90 by heterogeneous nucleation, leading to the formation of the ZIF-90@ZIF-8-A heterostructure.

To understand the interfacial interaction that drives the heterogeneous nucleation of ZIF-8 on ZIF-90, ZIF-90 was immersed in 2-MeIM solution, and then washed with methanol three times to remove free 2-MeIM physically adsorbed on surfaces and in frameworks. The solid sample was collected and labelled as ZIF-90/M. The FTIR spectrum of ZIF-90/M is presented in Fig. 5. The characteristic peak of C═O at 1675 cm^{-1} for ZIF-90 was retained after soaking in 2-MeIM solution. In addition, the appearance of a new peak at 1101 cm^{-1} (marked with a blue dashed line) and a shoulder at ~936 cm^{-1} (indicated by an arrow) suggests the

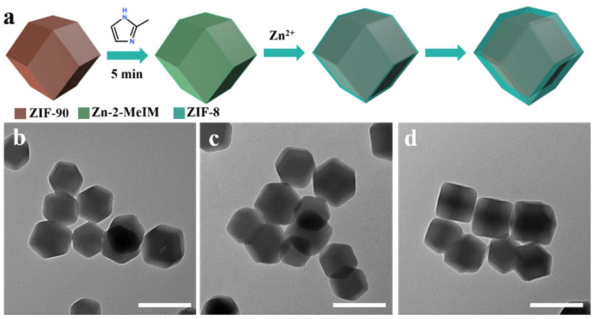

Fig. 4 (a) Schematic illustration of the synthesis of ZIF-90@ZIF-8-A. (b–d) TEM images of the intermediate sample collected during the synthesis of ZIF-90@ZIF-8-A at different reaction times of 2 min, 5 min and 20 min. The scale bar is 200 nm.

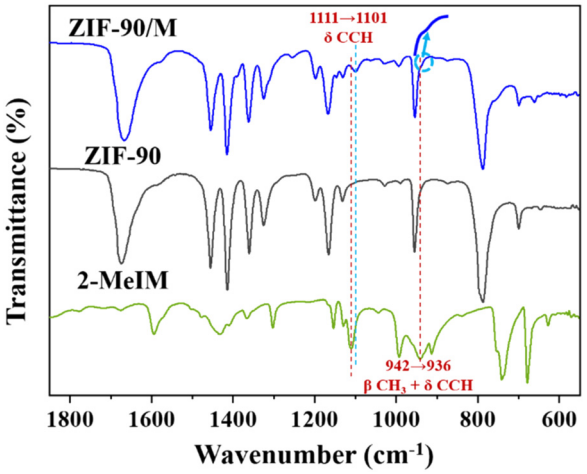

Fig. 5 FTIR spectrum of the ZIF-90/M sample obtained after soaking in 2-MeIM solution.

presence of 2-MeIM in ZIF-90/M. Compared with the corresponding peaks at 1111 cm^{-1} (C–C–H formation vibration) and 942 cm^{-1} ($-CH_3$ in-plane bending vibration and C–C–H formation vibration) of 2-MeIM (marked with a red dashed line),[42] these new peaks have a certain red shift. These observations suggest that the added 2-MeIM can coordinate with the exposed Zn central atoms on ZIF-90, causing the weakening of $-CH_3$ and C–C–H bonds.[43] Furthermore, our observation is in accordance with a literature report by Fan and co-workers. It is shown that the hydrolase-mimicking activity associated with the Zn–N node in ZIF-90 can be inhibited by acetate and EDTA,[44] suggesting that there exist coordination unsaturated Zn atoms in ZIF-90 that can bind to one of the two N atoms in the imidazole ring of the added 2-MeIM in our synthesis. Presumably, the subsequently added Zn^{2+} preferentially coordinates with the remaining N atom in the 2-MeIm bond to the ZIF-90 surface, leading to the heterogeneous nucleation of ZIF-8 on the ZIF-90 surface.

In the synthesis of ZIF-90@ZIF-8-B, Zn^{2+} was added into ZIF-90 solution under stirring for 5 min, and then 2-MeIM was introduced to allow ZIF-8 formation (Fig. 6a). After another 2 min of reaction, tiny nanoparticles with a diameter of about 27 nm appeared in the solution (Fig. 6b), indicating that ZIF-8 nanoparticles tend to form *via* homogeneous nucleation in methanol solution under such an addition sequence. With the increase of reaction time to 5 min, smaller-sized nanoparticles gradually adhered onto the surface of ZIF-90 (Fig. 6c). When the reaction time was prolonged to 20 min, ZIF-90@ZIF-8-B with a rough surface structure became dominant (Fig. 6d). Presumably, when Zn^{2+} was added first, ZIF-90 had no coordination effect on Zn^{2+}; thus, Zn^{2+} tended to interact with the later added 2-MeIM *via* homogeneous nucleation in solution, leading to the formation of ZIF-8 nanoparticles. It is suggested that there exists electrostatic interaction between the negatively charged ZIF-90 nanoparticles and positively charged ZIF-8 hosts;[45]

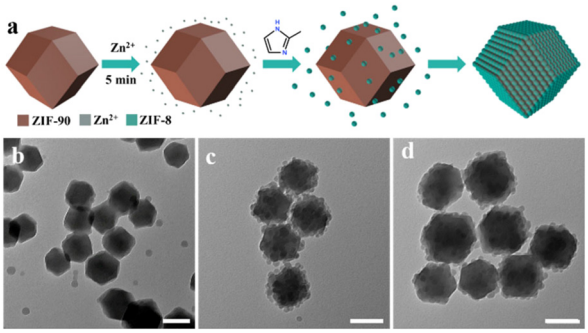

Fig. 6 (a) Schematic illustration of the synthesis of ZIF-90@ZIF-8-B. (b–d) TEM images of the intermediate sample collected during the synthesis of ZIF-90@ZIF-8-B at different reaction times of 2 min, 5 min and 20 min. The scale bar is 100 nm.

hence, core–satellite structure ZIF-90@ZIF-8-B with a rough surface is formed, which is different from core–shell structure ZIF-90@ZIF-8-A with a smooth surface.

Conclusions

In summary, we have demonstrated how to adjust heterogeneous and homogeneous nucleation for the structure regulation of ZIF-90@ZIF-8 hybrids. The nucleation mode of guest ZIF-8 is dependent on the addition sequence of metal ions and ligands in the presence of host ZIF-90. When 2-MeIM is introduced first, it will bond with the coordination unsaturated Zn atoms in ZIF-90 and trigger the heterogeneous nucleation and growth of ZIF-8 on ZIF-90, forming ZIF-90@ZIF-8-A with a core–shell structure and smooth surface. In contrast, when Zn^{2+} is added first, small ZIF-8 nanoparticles are formed first *via* homogeneous nucleation, and then adhere to the ZIF-90 surface and form ZIF-90@ZIF-8-B with a core–satellite structure and rough surface. This work presents a simple strategy for enriching the structural diversity of MOF-on-MOF materials.

Author contributions

Shumin Li performed the experiments. Shumin Li, Liang Zhao. Yining Yao, Zhengying Gu, Chao Liu, Wenli Hu, Ye Zhang, Qian Zhao and Chengzhong Yu conceived and designed the experiments, and analysed the results. Shumin Li wrote the manuscript. Liang Zhao and Chengzhong Yu revised the manuscript.

Conflicts of interest

There are no conflicts to declare.

Acknowledgements

The authors acknowledge the support from the National Natural Science Foundation of China (NSFC 21905092 and 22075085) and the Fundamental Research Funds for the Central Universities.

References

1 H. Furukawa, K. E. Cordova, M. O'Keeffe and O. M. Yaghi, *Science*, 2013, **341**, 974.
2 H. C. Zhou, J. R. Long and O. M. Yaghi, *Chem. Rev.*, 2012, **112**, 673–674.
3 H. C. Zhou and S. Kitagawa, *Chem. Soc. Rev.*, 2014, **43**, 5415–5418.
4 A. C. McKinlay, R. E. Morris, P. Horcajada, G. Ferey, R. Gref, P. Couvreur and C. Serre, *Angew. Chem., Int. Ed.*, 2010, **49**, 6260–6266.
5 B. Li, H. M. Wen, Y. J. Cui, W. Zhou, G. D. Qian and B. L. Chen, *Adv. Mater.*, 2016, **28**, 8819–8860.
6 H. Furukawa and O. M. Yaghi, *J. Am. Chem. Soc.*, 2009, **131**, 8875–8883.
7 S. Begum, Z. Hassan, S. Brase, C. Woll and M. Tsotsalas, *Acc. Chem. Res.*, 2019, **52**, 1598–1610.
8 J. Yang and Y. W. Yang, *Small*, 2020, **16**, 1906846.
9 J. R. Zhou, G. Tian, L. J. Zeng, X. E. Song and X. W. Bian, *Adv. Healthcare Mater.*, 2018, **7**, 1800022.
10 M. X. Wu and Y. W. Yang, *Adv. Mater.*, 2017, **29**, 1606134.
11 P. Horcajada, R. Gref, T. Baati, P. K. Allan, G. Maurin, P. Couvreur, G. Ferey, R. E. Morris and C. Serre, *Chem. Rev.*, 2012, **112**, 1232–1268.
12 Z. Chang, D. H. Yang, J. Xu, T. L. Hu and X. H. Bu, *Adv. Mater.*, 2015, **27**, 5432–5441.
13 T. Simon-Yarza, A. Mielcarek, P. Couvreur and C. Serre, *Adv. Mater.*, 2018, **30**, 1707365.
14 Y. F. Gu, Y. N. Wu, L. C. Li, W. Chen, F. T. Li and S. Kitagawa, *Angew. Chem., Int. Ed.*, 2017, **56**, 15658–15662.
15 M. S. Yao, J. W. Xiu, Q. Q. Huang, W. H. Li, W. W. Wu, A. Q. Wu, L. A. Cao, W. H. Deng, G. E. Wang and G. Xu, *Angew. Chem., Int. Ed.*, 2019, **58**, 14915–14919.
16 X. Qiu, W. Zhong, C. H. Bai and Y. W. Li, *J. Am. Chem. Soc.*, 2016, **138**, 1138–1141.
17 K. S. Park, Z. Ni, A. P. Cote, J. Y. Choi, R. D. Huang, F. J. Uribe-Romo, H. K. Chae, M. O'Keeffe and O. M. Yaghi, *Proc. Natl. Acad. Sci. U. S. A.*, 2006, **103**, 10186–10191.
18 X. C. Huang, Y. Y. Lin, J. P. Zhang and X. M. Chen, *Angew. Chem., Int. Ed.*, 2006, **45**, 1557–1559.
19 C. H. Kuo, Y. Tang, L. Y. Chou, B. T. Sneed, C. N. Brodsky, Z. P. Zhao and C. K. Tsung, *J. Am. Chem. Soc.*, 2012, **134**, 14345–14348.
20 G. Li, W. H. Deng, L. He, J. Y. Wu, J. C. Liu, T. J. Wu, Y. Wang and X. Y. Wang, *ACS Appl. Mater. Interfaces*, 2021, **13**, 28324–28333.
21 W. H. Deng, G. Li, T. J. Wu, L. He, J. Y. Wu, J. C. Liu, H. T. Zheng, X. L. Li, Y. Q. Yang, M. J. Jing, Y. Wang and X. Y. Wang, *Carbon*, 2022, **186**, 589–598.
22 K. Jayaramulu, K. K. R. Datta, C. Rosler, M. Petr, M. Otyepka, R. Zboril and R. A. Fischer, *Angew. Chem., Int. Ed.*, 2016, **55**, 1178–1182.
23 T. Yoon, T. Bok, C. Kim, Y. Na, S. Park and K. S. Kim, *ACS Nano*, 2017, **11**, 4808–4815.
24 W. Morris, C. J. Doonan, H. Furukawa, R. Banerjee and O. M. Yaghi, *J. Am. Chem. Soc.*, 2008, **130**, 12626.

25 T. Jose, Y. Hwang, D. W. Kim, M. I. Kim and D. W. Park, *Catal. Today*, 2015, **245**, 61–67.
26 D. Mo, Z. Q. Wang, K. Y. Sun, X. Y. Xie, J. X. Zhang and K. Y. Cai, *J. Mater. Chem. C*, 2020, **8**, 11110–11118.
27 C. Liu, J. Wang, J. J. Wan and C. Z. Yu, *Coord. Chem. Rev.*, 2021, **432**, 213743.
28 S. Choi, T. Kim, H. Ji, H. J. Lee and M. Oh, *J. Am. Chem. Soc.*, 2016, **138**, 14434–14440.
29 C. Liu, L. N. Lin, Q. Sun, J. Wang, R. Huang, W. Y. Chen, S. M. Li, J. J. Wan, J. Zou and C. Z. Yu, *Chem. Sci.*, 2020, **11**, 3680–3686.
30 M. T. Zhao, J. Z. Chen, B. Chen, X. Zhang, Z. Y. Shi, Z. Q. Liu, Q. L. Ma, Y. W. Peng, C. L. Tan, X. J. Wu and H. Zhang, *J. Am. Chem. Soc.*, 2020, **142**, 8953–8961.
31 G. Lee, S. Lee, S. Oh, D. Kim and M. Oh, *J. Am. Chem. Soc.*, 2020, **142**, 3042–3049.
32 T. H. Bae, J. S. Lee, W. L. Qiu, W. J. Koros, C. W. Jones and S. Nair, *Angew. Chem., Int. Ed.*, 2010, **49**, 9863–9866.
33 W. S. Chi, S. Hwang, S. J. Lee, S. Park, Y. S. Bae, D. Y. Ryu, J. H. Kim and J. Kim, *J. Membr. Sci.*, 2015, **495**, 479–488.
34 D. C. Mei, H. Li, L. J. Liu, L. C. Jiang, C. H. Zhang, X. R. Wu, H. X. Dong and F. Q. Ma, *Chem. Eng. J.*, 2021, **425**, 130468.
35 E. E. Sann, Y. Pan, Z. F. Gao, S. S. Zhan and F. Xia, *Sep. Purif. Technol.*, 2018, **206**, 186–191.
36 W. F. Wu, J. Y. Su, M. M. Jia, Z. J. Li, G. Q. Liu and W. B. Li, *Sci. Adv.*, 2020, **6**, eaax7270.
37 Y. Pan, K. A. Sun, S. J. Liu, X. Cao, K. L. Wu, W. C. Cheong, Z. Chen, Y. Wang, Y. Li, Y. Q. Liu, D. S. Wang, Q. Peng, C. Chen and Y. D. Li, *J. Am. Chem. Soc.*, 2018, **140**, 2610–2618.
38 K. Koh, A. G. Wong-Foy and A. J. Matzger, *Chem. Commun.*, 2009, 6162–6164, DOI: **10.1039/b904526k**.
39 X. G. Wang, L. Xu, M. J. Li and X. Z. Zhang, *Angew. Chem., Int. Ed.*, 2020, **59**, 18078–18086.
40 A. U. Ortiz, A. P. Freitas, A. Boutin, A. H. Fuchs and F. X. Coudert, *Phys. Chem. Chem. Phys.*, 2014, **16**, 9940–9949.
41 W. B. Liang, H. S. Xu, F. Carraro, N. K. Maddigan, Q. W. Li, S. G. Bell, D. M. Huang, A. Tarzia, M. B. Solomon, H. Amenitsch, L. Vaccari, C. J. Sumby, P. Falcaro and C. J. Doonan, *J. Am. Chem. Soc.*, 2019, **141**, 2348–2355.
42 A. Di Santo, H. Pérez, G. A. Echeverría, O. E. Piro, R. A. Iglesias, R. E. Carbonio, A. B. Altabef and D. M. Gil, *RSC Adv.*, 2018, **8**, 23891–23902.
43 Sabad-e-Gul, S. Waheed, A. Ahmad, S. M. Khan, M. Hussain, T. Jamil and M. Zuber, *J. Taiwan Inst. Chem. Eng.*, 2015, **57**, 129–138.
44 C. Y. Fan, Y. H. Tang, H. Wang, Y. F. Huang, F. Xu, Y. Yang, Y. Y. Huang, W. F. Rong and Y. H. Lin, *Nanoscale*, 2022, **14**, 7985–7990.
45 Z. Q. Jiang, Y. J. Wang, L. Sun, B. Yuan, Y. C. Tian, L. C. Xiang, Y. Y. Li, Y. Li, J. Li and A. G. Wu, *Biomaterials*, 2019, **197**, 41–50.